# • Electronic Supplementary Information (ESI)

# Quantum Sieving of $H_2/D_2$ in MOFs: A Study on the Correlation between the Separation Performance, Pore Size and Temperature

Dawei Cao,‡[a,b] Jiahao Ren,‡[c] Yu Gong,[b] Hongliang Huang,[d] Xiaolong Fu,[b] Miao Chang,[c] Xiaojun Chen,[b] Chengjian Xiao,[b] Dahuan Liu,[c] Qingyuan Yang,*[c] Chongli Zhong,[d] Shuming Peng*[b] and Zhengjun Zhang*[a,e]

[a.] *Department of Engineering Physics, Tsinghua University, Beijing 100084, P. R. China. Email: zjzhang@tsinghua.edu.cn*

[b.] *Institute of Nuclear Physics and Chemistry, China Academy of Engineering Physics, Mianyang, Sichuan 621900, P. R. China. Email: pengshuming@caep.cn*

[c.] *State Key Laboratory of Organic–Inorganic Composites; Beijing Advanced Innovation Center for Soft Matter Science and Engineering, Beijing University of Chemical Technology, Beijing 100029, P. R. China. Email: qyyang@mail.buct.edu.cn*

[d.] *State Key Laboratory of Separation Membranes and Membrane Processes, Tianjin Polytechnic University, Tianjin 300387, P. R. China.*

[e.] *Advanced Materials Laboratory, Department of Materials Science and Engineering, Tsinghua University, Beijing 100084, P. R. China.*

‡*These authors contributed equally.*

# TABLE OF CONTENTS

## Section1: Preparation and characterization of the three MOF materials

### S1.1 Preparation

All starting chemical reagents and solvents employed in this work were commercially available and used as supplied without further purification.

**MOF-EIA.**[1] 0.1 mmol (24.1 mg) of $Cu(NO_3)_2 \cdot 6H_2O$ and 0.2 mmol (42.1 mg) of 5-ethoxy isophthalic acid (5-EIA) were dissolved in a solvent of 4 mL DMF+0.5 mL $H_2O$ in a 15 mL glass vial (one batch). The vials were then capped and placed at 90 °C in a hot air oven for 24 hrs, afterwards, blue-colored crystals were collected and washed with the mother solvent mixture, the crystals were dried under reduced pressure for 12 hrs, then were treated with a measured amount of DI water (50 mL/mg) under stirring, the crystals turn opaque upon the addition of DI water. After 10 mins' stirring, the crystals of MOF-EIA were collected by filtration, followed by another 2 hrs' drying under reduced pressure.

**CPL-1.**[2, 3] A solution (solution A) of $Na_2pzdc$ (0.21 g, 1.00 mmol, pzdc=pyrazine-2,3-dicarboxylate) in $H_2O$ (20 mL) was slowly added to the $H_2O$ solution (solution B, 20 mL) containing $Cu(ClO_4)_2 \cdot 6H_2O$ (0.37 g, 1.00 mmol) and pyrazine (1.0 g, 12.5 mmol) under stirring, blue microcrystals obtained were collected by filtration after a few minutes, the crystals were dried under reduced pressure for 2 hrs.

**ZIF-8.**[4] ZIF-8 was synthesized in a purely aqueous system: firstly, 1.17 g $Zn(NO_3)_2 \cdot 6H_2O$ was dissolved in 8 ml deionized (DI) water (solution A); secondly, 22.70 g 2-methylimidazole was dissolved in another 80 ml DI water (solution B); then solution A was mixed with solution B under stirring. All the operations were performed at room temperature, the synthesis solution turned milky instantly upon mixing of the two solutions. After stirring for ~5 mins, the product was collected by repeated centrifugation and washed with DI water for three times, the product was dried at 65 ℃ under reduced pressure for 2 hrs.

### S1.2 Characterization

**PXRD**

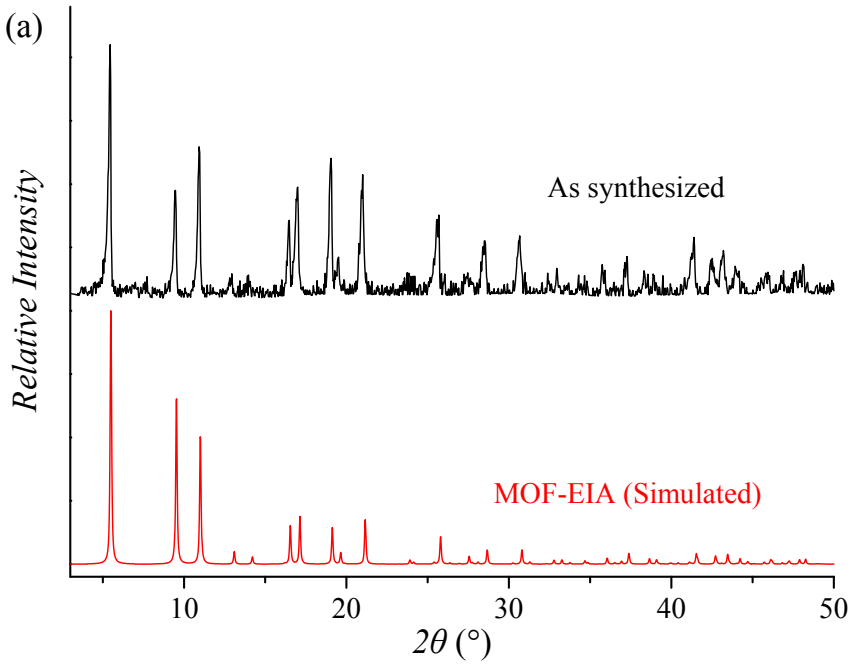

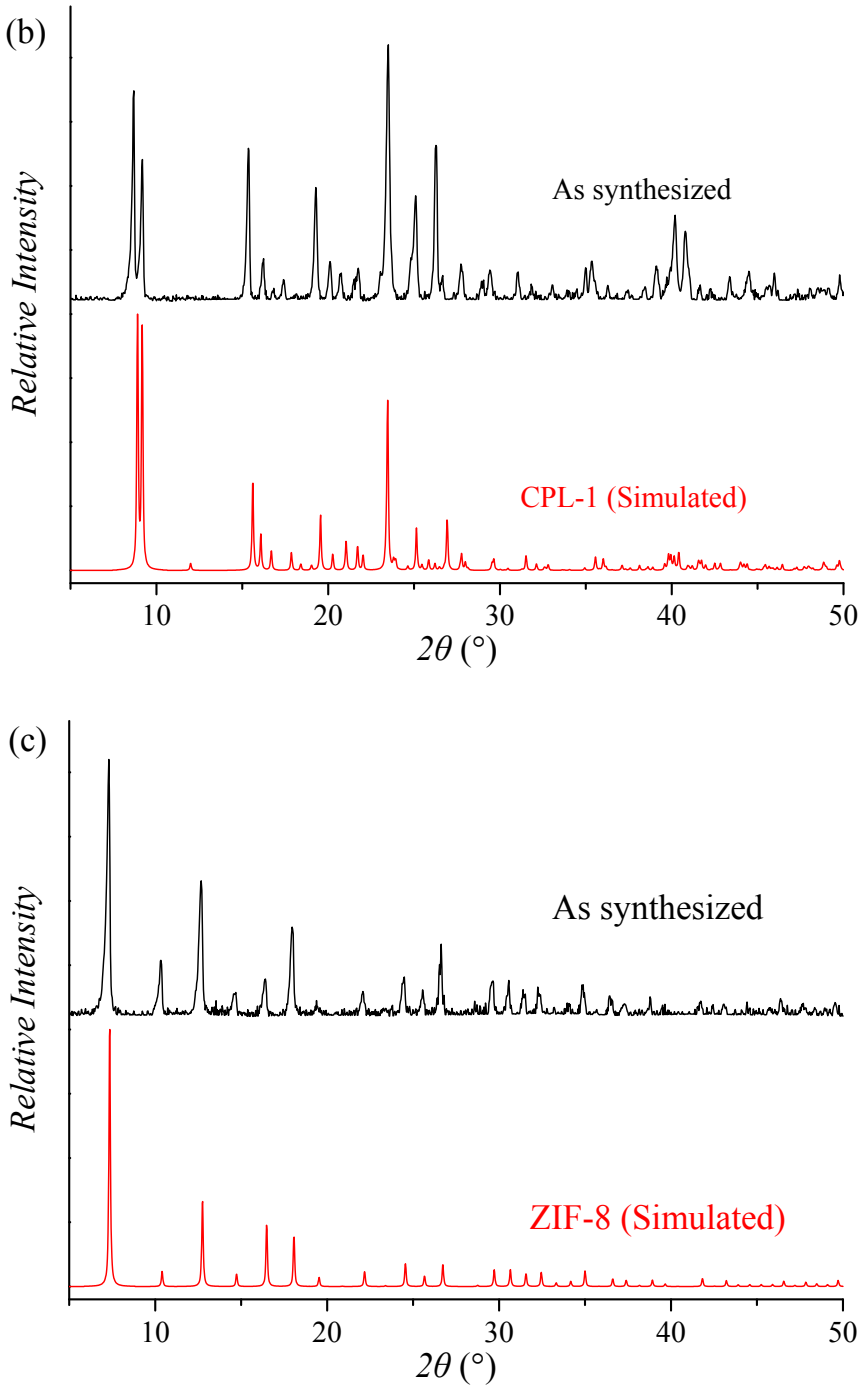


**Figure S1.** Comparison of simulated and experimental PXRD patterns of (a) MOF-EIA, (b) CPL-1 and (c) ZIF-8.

**FTIR**

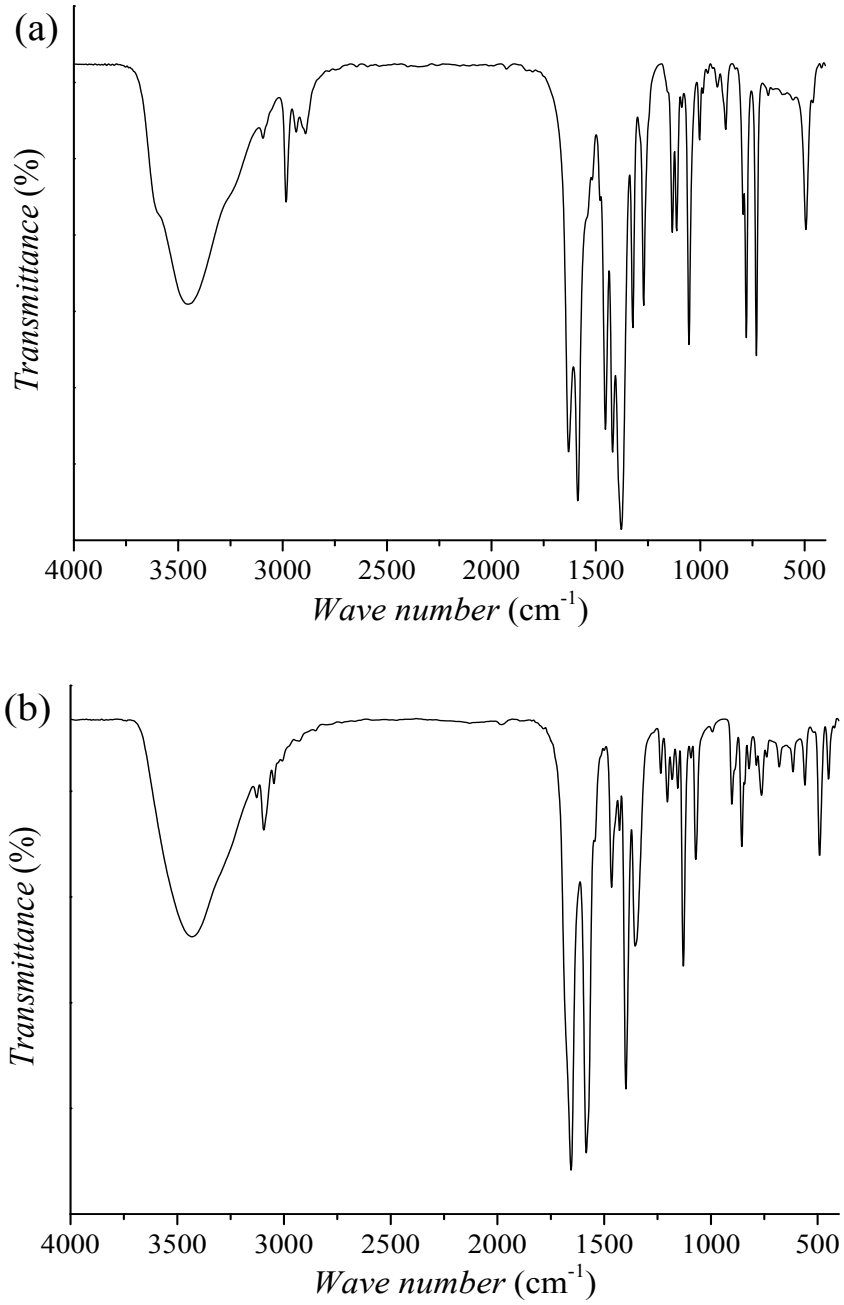
(a)
Transmittance (%)
4000
3500
3000
2500
2000
1500
1000
500
Wave number (cm-1)
(b)
Transmittance (%)
4000
3500
3000
2500
2000
1500
1000
500
Wave number (cm-1)

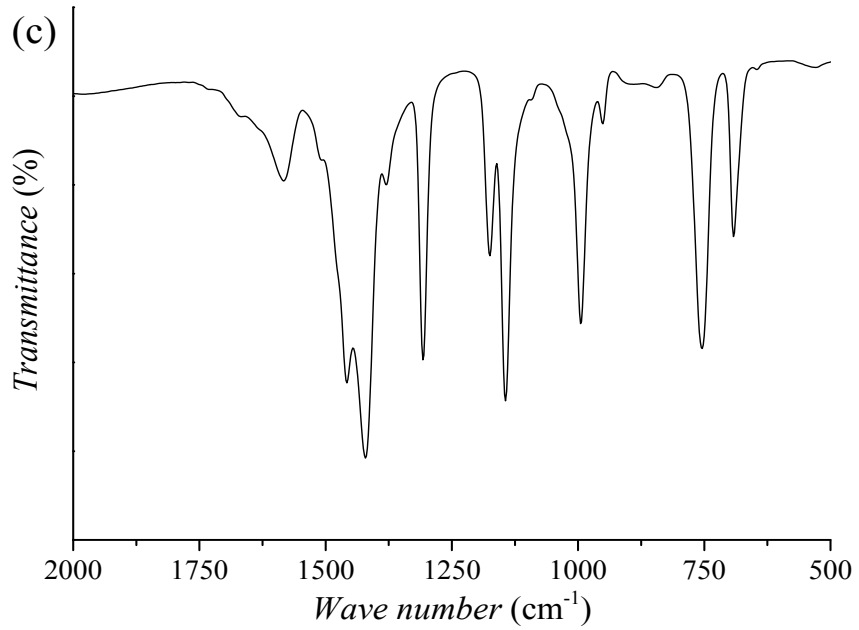


**Figure S2.** The FTIR spectra of as-synthesized (a) MOF-EIA, (b) CPL-1 and (c) ZIF-8.

**TGA**

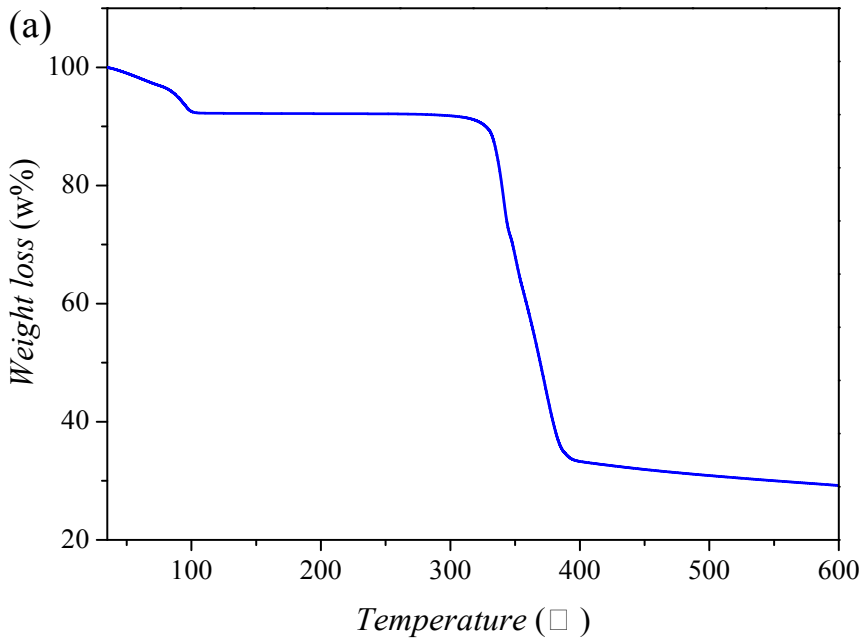

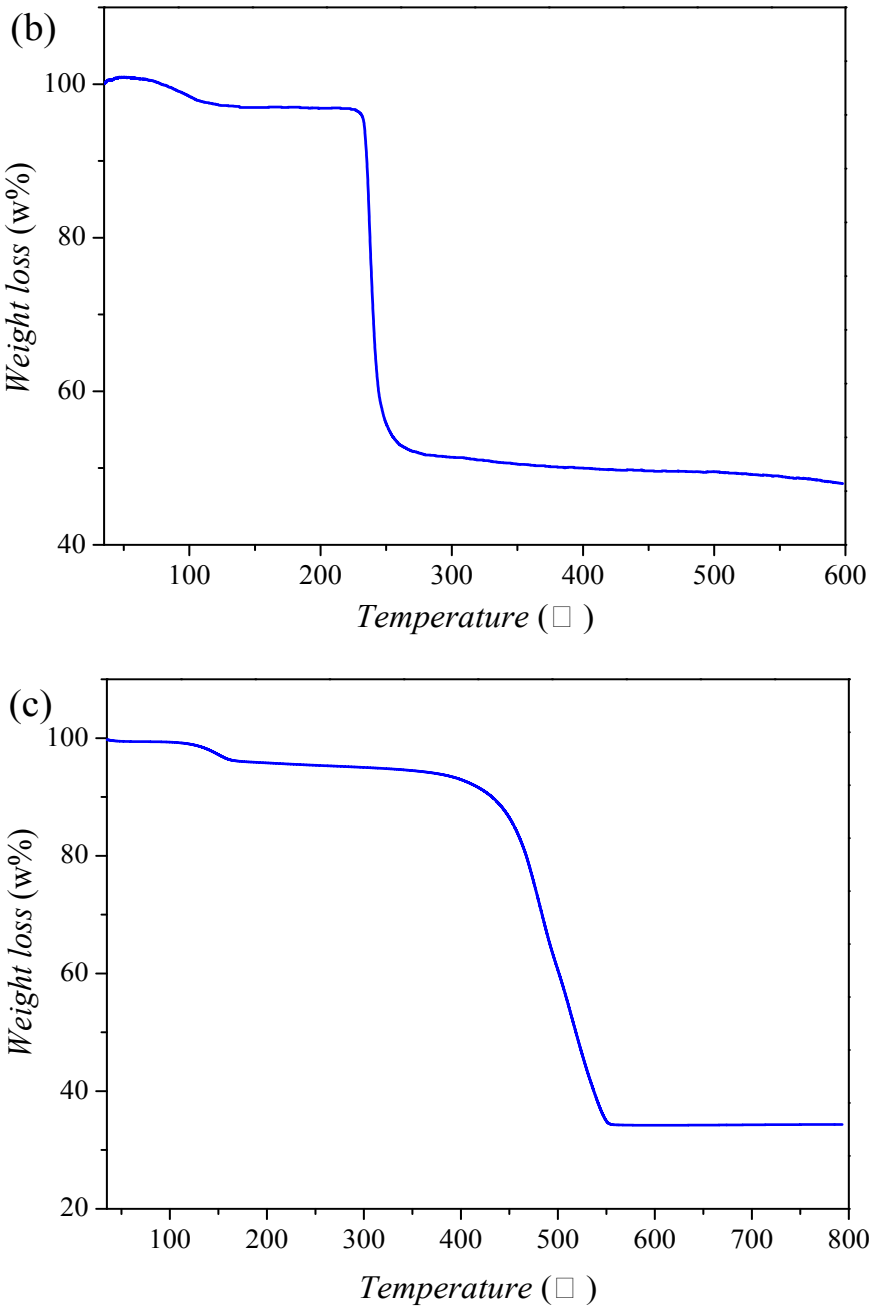


**Figure S3.** TGA trace of as-synthesized (a) MOF-EIA, (b) CPL-1 and (c) ZIF-8.

**$N_2$ isotherms at 77 K**

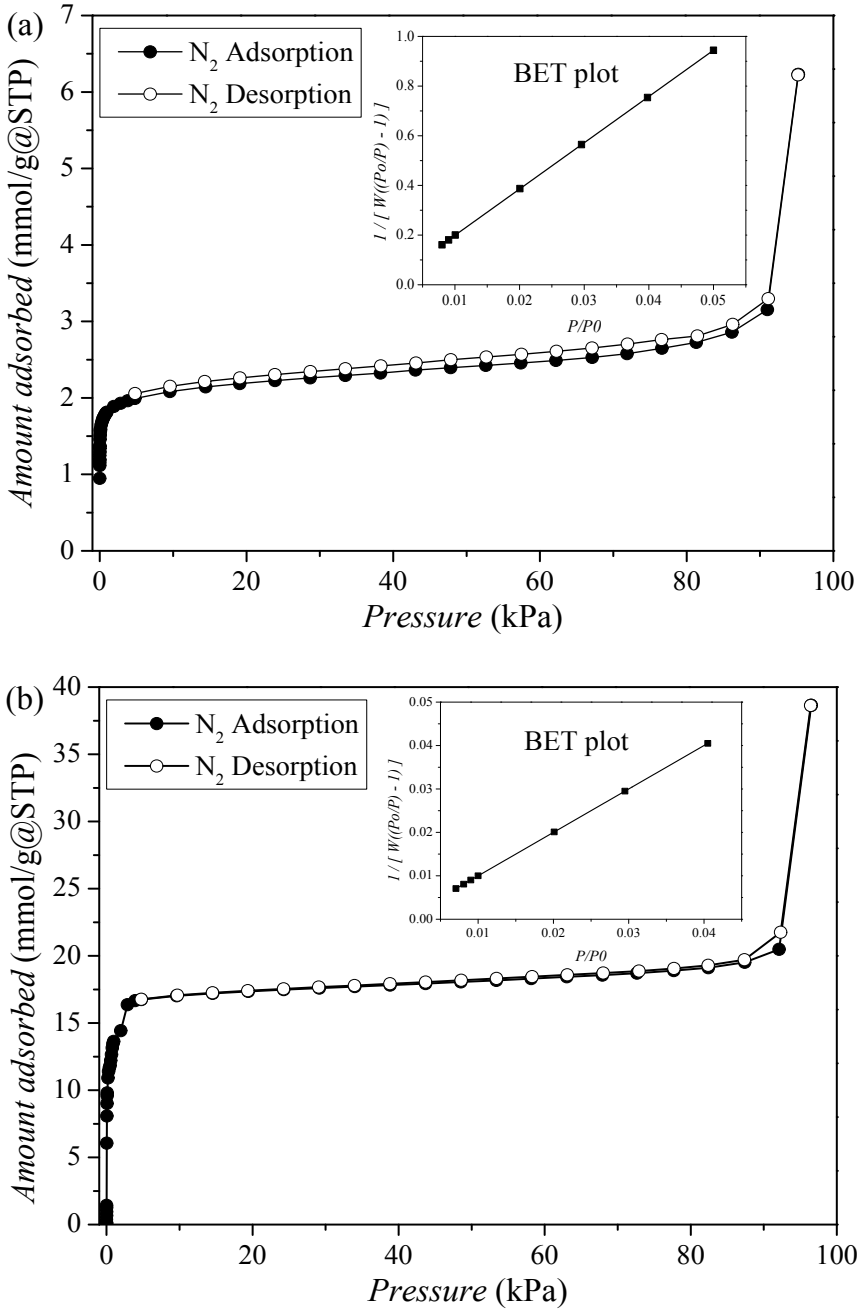


**Figure S4.** $N_2$ isotherms at 77 K for as-synthesized (a) MOF-EIA and (b) ZIF-8. The BET plots were also shown in the inlets. (Note that for CPL-1, $N_2$ adsorption at 77 K couldn't be performed)

## Section 2. Advanced cryogenic thermal desorption spectroscopy (ACTDS) apparatus and temperature-programmed desorption (TPD) methodology

### S2.1 ACTDS apparatus

Figure S5a shows our ACTDS apparatus used for the quantum sieving investigations of equimolar $D_2/H_2$

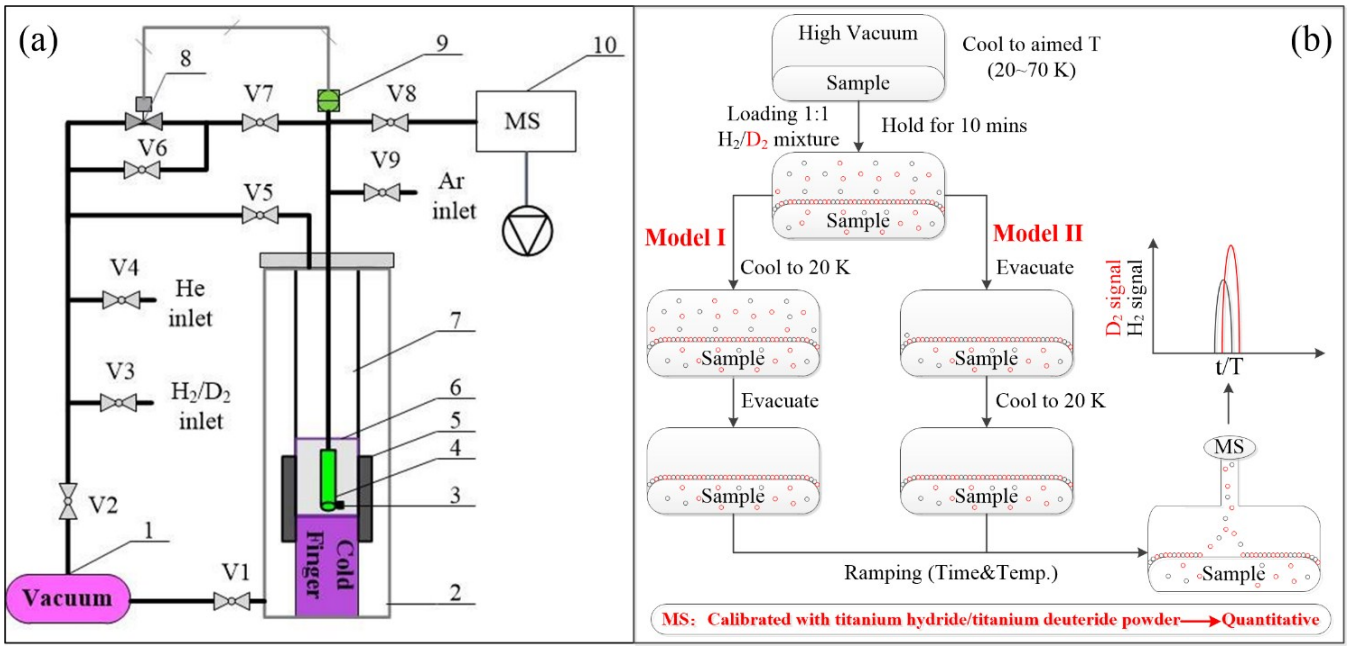


**Figure S5.** (a) Schematic of our ACTDS apparatus. (b) Two models in TPD methodology for the quantum sieving of $D_2/H_2$ mixtures.

mixture, details about which was presented elsewhere.[5]

### S2.2 TPD methodology

Temperature-programmed desorption (TPD) or thermal-desorption spectroscopy (TDS) is a methodology most commonly used in surface and analytical chemistry.[6-10] However, it could also be used as an efficient separation method. The group of Michael Hirscher first applied TPD methodology into the $H_2/D_2$ quantum sieving investigations, for the first time realized the direct measurement of the separation of a real $D_2/H_2$ mixture.[11] Moreover, by using the TPD methodology, investigations on the separation of $D_2/H_2$ through quantum sieving run into promising prospects.[12, 13]

As proposed in literature, there are two models within TPD methodology as shown in figure S5b, depending on the properties of the materials investigated. For materials possessing strong diffusion limitation effect, it suits model I; for materials possessing strong binding site but no diffusion limitation, model II suits.[12, 13] Both models are proved appropriate in $D_2/H_2$ quantum sieving investigations[15, 16] and for the investigation in this study, we applied both models depending on different materials.

$D_2/H_2$ quantum sieving with model II on our ACTDS apparatus was already described elsewhere,[5, 17] so here we just describe our $D_2/H_2$ quantum sieving with model I on CPL-1: first, CPL-1 (milligram in weight) having been activated for 12 hr at 120 ℃ under high vacuum (final pressure $<10^{-4}$ Pa) in the sample chamber was cooled down to the experimental temperature (20 K, 30 K, 40 K and 50 K) under high vacuum; then, a defined pressure (0.5 kPa, 1.0 kPa, 3.0 kPa and 5.0 kPa) of equimolar $D_2/H_2$ mixture was dosed into the sample chamber and held there for 10 min; afterwards, the sample was cooled down

to a temperature lower than 20 K where the remaining gas molecules are pumped off until a high vacuum is reached again—as adsorption may also occur during the cooling process, the cooling process needs to be done fast in case of affecting the adsorption equilibrium to a large scale (and that is why we only carry it out to a temperature of 50 K, where a cooling time of slightly larger than 1 min is guaranteed); finally, the thermally activated desorption procedure was initiated with a simultaneous recording of the desorbed $D_2/H_2$ signal by a calibrated quadrupole MS, which, can give out a quantified amount of the desorbed $D_2/H_2$ gases (right proportional to the area under the desorption curve).[9] While, as the sample chamber of our ACTDS apparatus is suspended in a pure helium environment as presented before,[5] the heating ramp of the thermally activated desorption procedure is not rigorously linear.

## Section 3. The TPD spectra and $D_2/H_2$ selectivity (EF, enrichment factor)

### S3.1 The TPD spectra of the three MOF materials

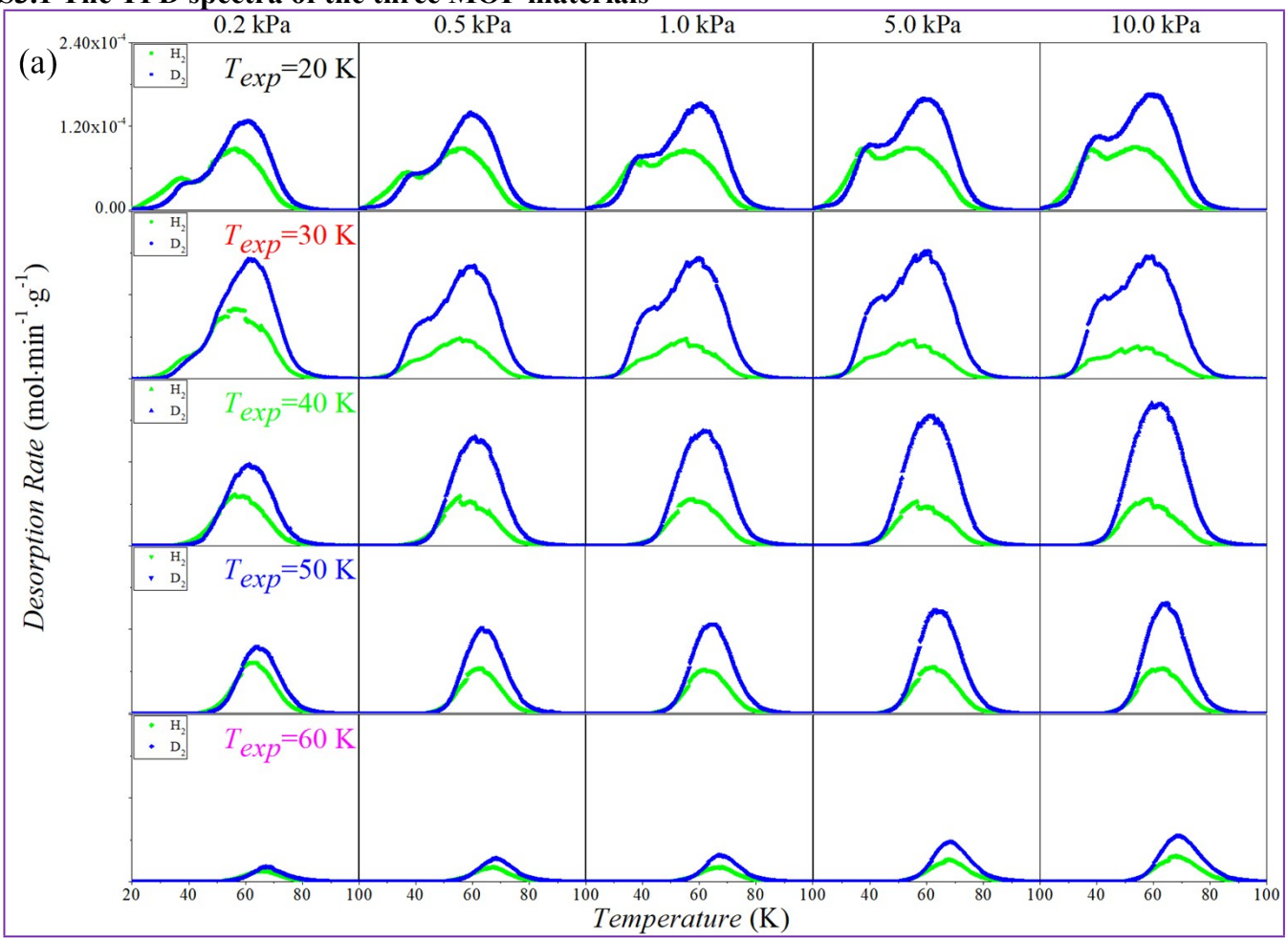

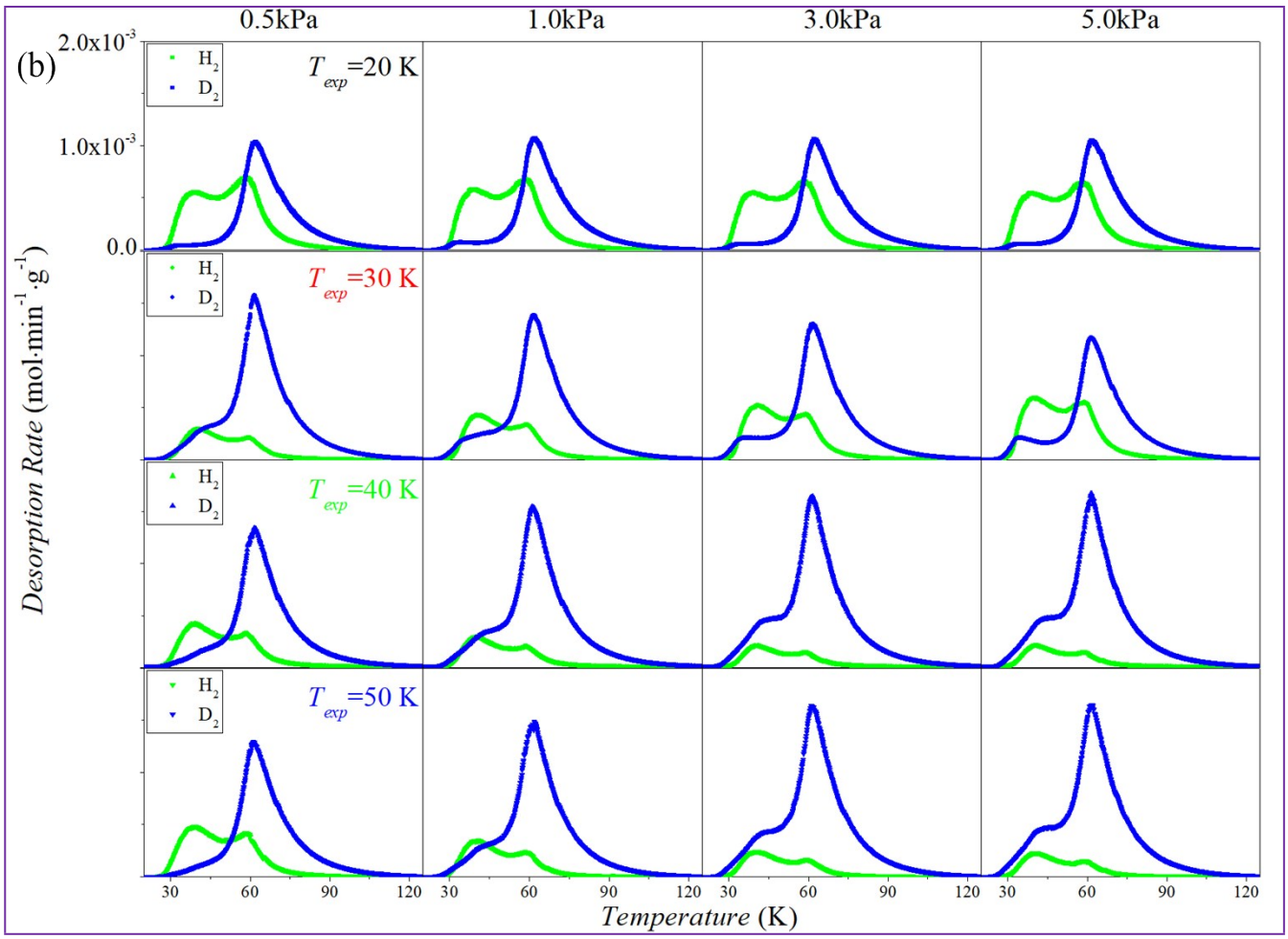
(b)
0.5kPa
1.0kPa
3.0kPa
5.0kPa
2.0x10-3
1.0x10-3
0.0
H2
D2
Texp=20 K
Texp=30 K
Texp=40 K
Texp=50 K
Desorption Rate (mol·min-1·g-1)
30
60
90
120
Temperature (K)

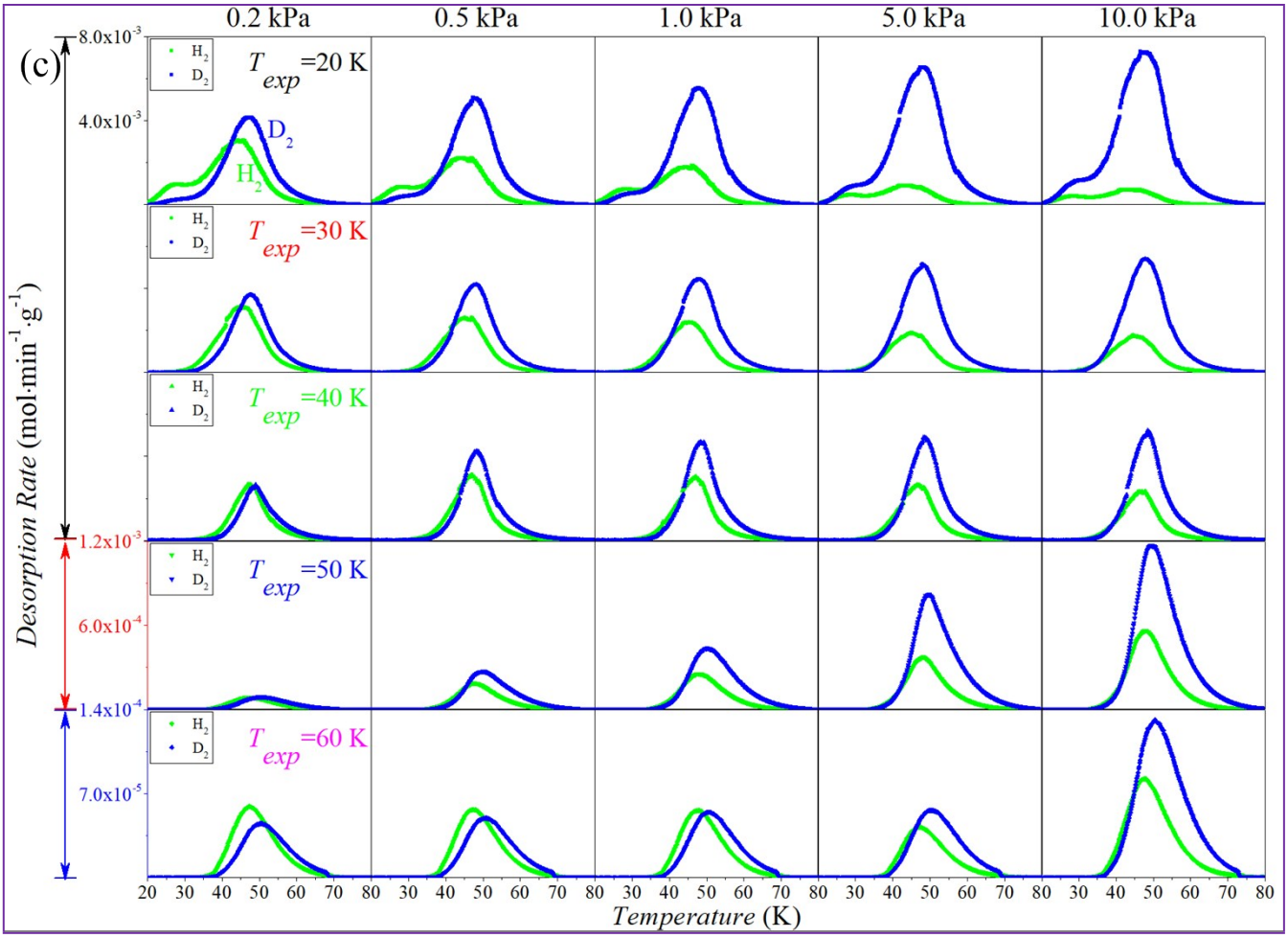


**Figure S6.** Equimolar $H_2$ (green)/$D_2$ (blue) TPD spectra (with non-rigorous linear ramping rate) of (a) MOF-EIA, (b) CPL-1 and (c) ZIF-8 at different loading pressures (0.2~10.0 kPa) and different exposure temperatures: 20 K (■), 30 K (●), 40 K (▲), 50 K (▼) and 60 K (◆).

### S3.2 $D_2/H_2$ selectivity/EF on the three MOF materials

Equimolar $D_2/H_2$ selectivity/EF was deduced from $n_{D_2}/n_{H_2}$ with $n_{D_2}$ and $n_{H_2}$ the adsorbed amounts of $D_2$ and $H_2$ respectively.

**Table S1**. Equimolar $D_2/H_2$ selectivity/EF of material MOF-EIA at given exposure temperatures and loading pressures.

| **Pressure (kPa)** | **Selectivity/EF ($n_{D_2}/n_{H_2}$)** | | | | |
|---|---|---|---|---|---|
| | **20 K** | **30 K** | **40 K** | **50 K** | **60 K** |
| **0.5** | 1.36 | 2.05 | 1.64 | 1.37 | 1.33 |
| **1.0** | 1.43 | 3.02 | 2.39 | 2.00 | 1.63 |
| **3.0** | 1.61 | 3.46 | 2.62 | 2.12 | 1.80 |
| **5.0** | 1.62 | 3.69 | 3.23 | 2.32 | 1.87 |
| **10.0** | 1.72 | 4.01 | 3.31 | 2.44 | 1.86 |

**Table S2**. Equimolar $D_2/H_2$ selectivity/EF of material CPL-1 at given exposure temperatures and loading pressures.

| Pressure (kPa) | Selectivity/EF ($^{n_{D_2}}/_{n_{H_2}}$) | | | |
|---|---|---|---|---|
| | **20 K** | **30 K** | **40 K** | **50 K** |
| **0.5** | 1.33 | 5.56 ± 0.02 | 3.12 | 2.42 |
| **1.0** | 1.42 | 3.83 ± 0.36 | 5.90 | 4.84 |
| **3.0** | 1.42 | 2.45 ± 0.11 | 9.22 | 7.77 |
| **5.0** | 1.44 | 2.00 ± 0.11 | 9.25 | 8.61 |

**Table S3**. Equimolar $D_2/H_2$ selectivity/EF of material ZIF-8 at given exposure temperatures and loading pressures.

| Pressure (kPa) | Selectivity/EF ($^{n_{D_2}}/_{n_{H_2}}$) | | | | |
|---|---|---|---|---|---|
| | **20 K** | **30 K** | **40 K** | **50 K** | **60 K** |
| **0.2** | 1.19 | 1.01 | 1.03 | 1.18 | 0.87 |
| **0.5** | 1.92 | 1.57 | 1.37 | 1.66 | 1.00 |
| **1.0** | 2.61 | 1.87 | 1.57 | 1.93 | 1.11 |
| **5.0** | 6.03 | 2.76 | 1.84 | 2.42 | 1.45 |
| **10.0** | 8.36 | 3.20 | 2.21 | 2.33 | 1.80 |

Please note values in boxes (where an obvious different trend was observed) were calculated with repeated measurements.

## Section 4. Simulations on the material of MOF-EIA

### S4.1 Fine structure of MOF-EIA

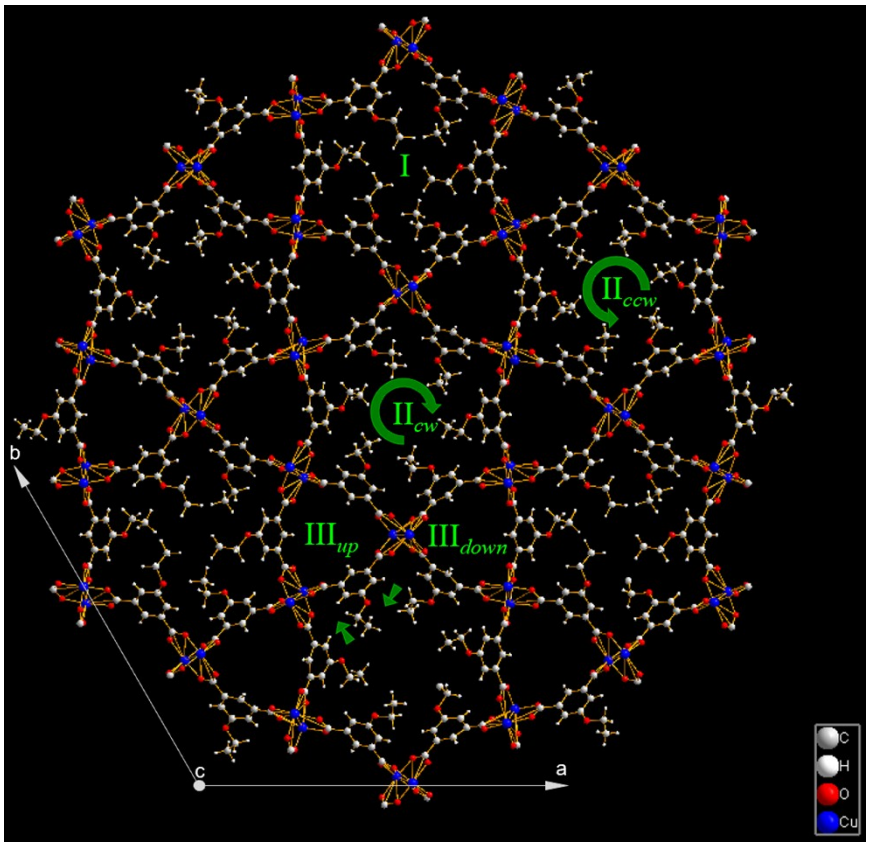


**Figure S7.** Fine schematic view of the crystal structure of MOF-EIA. In fact, there exist three types of pores which can be further divided into five sub-types: the hexagonal pore with disordered ethyl groups (I), whose mouth is too small [0.66×0.66 Å] for the adsorption of $H_2/D_2$ (see Figure S8 below); the hexagonal pore with ordered ethyl groups distributed clockwise ($II_{cw}$) and counter-clockwise ($II_{ccw}$); the triangular pore with the ethyl groups on its sides pointing upwards ($III_{up}$) and downwards ($III_{down}$). The hexagonal pores with ordered ethyl groups ($II_{cw}$ and $II_{ccw}$) are structural identical once one looks from the opposite side, so do the triangular ones ($III_{up}$ and $III_{down}$). Calculation work was based on this fine structure of MOF-EIA.

### S4.2 Simulation details

To qualitatively understand the influence of the textural characteristics of materials on the correlation revealed, Monte Carlo simulations in the canonical ensemble (NVT-MC) were performed to explore the microscopic co-adsorption mechanisms of $D_2$ and $H_2$ molecules in MOF-EIA, using our in-house code HT-CADSS. The loadings used in these calculations were obtained from grand canonical Monte Carlo (GCMC) simulations that were performed on the $D_2/H_2$ mixture with equimolar bulk composition, under the conditions of 10 kPa and different temperatures. In our calculations, the MOF framework was considered to be rigid with periodic boundary conditions along all the three dimensions. A combination of Lennard-Jones (LJ) and Columbic potentials was used to describe the adsorbate-adsorbate and adsorbate-MOF interactions. To account for the quantum effect of hydrogen isotope adsorption at low temperatures, quartic Feynman-Hibbs effective potential was adopted using the formula revised by Rodríguez-Cantano et al.[18] $D_2$ and $H_2$ molecules were represented using the model proposed by Darkrim and Levesque.[19] The LJ parameters for the MOF framework atoms were taken from DREIDING force field,[20] and their density derived electrostatic and chemical (DDEC)[21] charges were derived from density

functional theory (DFT) calculation using the VASP code (version 5.3.5).[22, 23] A cut-off distance of 14 Å was used to calculate all the van deer Waals (VDW) type interactions and the long-range Coulombic interactions were handled using the Ewald summation method. For GCMC and NVT-MC simulations, each run was performed with $1 \times 10^7$ steps for system equilibration with another $1 \times 10^7$ steps for statistical average. During each NVT-MC run, the adsorption configurations of the $D_2/H_2$ mixtures in the MOF were sampled at an interval of 2000 steps during the production stage. The results were subsequently employed to examine the center of mass (COM) probability distributions of the adsorbate molecules and the microscopic selectivity distribution of $D_2$ over $H_2$ in the MOF-EIA structure. The definition of microscopic selectivity and the calculation method can be found in our previous work.[24]

It should be pointed out that the DFT-optimized period structure of MOF-EIA was used for all of the calculations involved in this work (Figure S7). The structure was optimized until the forces on all atoms were smaller than 0.03 eV/Å and the SCF convergence criteria is below $5 \times 10^{-5}$ eV. A plane-wave basis set with an energy cut-off of 600 eV was employed, along with the Perdew-Burke-Ernzerhof (PBE) exchange-correlation functional.[24] The long-range weak dispersion interactions were taken into account by DFT D3 van der Waals interaction correction method.[26] The electron-ion interactions were described by the projector augmented wave (PAW)[27] method in the implementation of Kresse and Joubert.[28] The Brillouin zone integration was performed using a $(1 \times 1 \times 6)$ Monkhorst-Pack grid.[29]

The MOF-EIA structure is very complex in which there are three types of pores with different pore sizes, as shown in Figure S7. During our MC simulations, the type-I pores were artificially blocked because they are inaccessible to $D_2$ and $H_2$ molecules. For demonstrate the necessity of such treatment, molecular dynamics (MD) simulations in the NVT ensemble were performed for pure $H_2$ and $D_2$ gases by only inserting one molecule in the type-I pore, at the highest temperature (60 K) examined in this work. The velocity-Verlet algorithm[30] was used to integrate the Newton's equation of motion with the NO_SQUISH scheme[31] for rotational movement. A Nosé-Hoover chain thermostat[30] was used to maintain the systems under constant-temperature condition. The time step was set to 0.5 fs and the MD simulation duration was 3.5 ns with the last 2.5 ns for production. Figure S8 shows the mean square displacements (MSD) of $H_2$ and $D_2$ molecules derived from MD simulations. Obviously, the adsorbate molecules are tightly trapped in the type-I pore which cannot move out within so long simulation time considered here. These observations indicate that $D_2$ and $H_2$ cannot enter into such types in real situations.

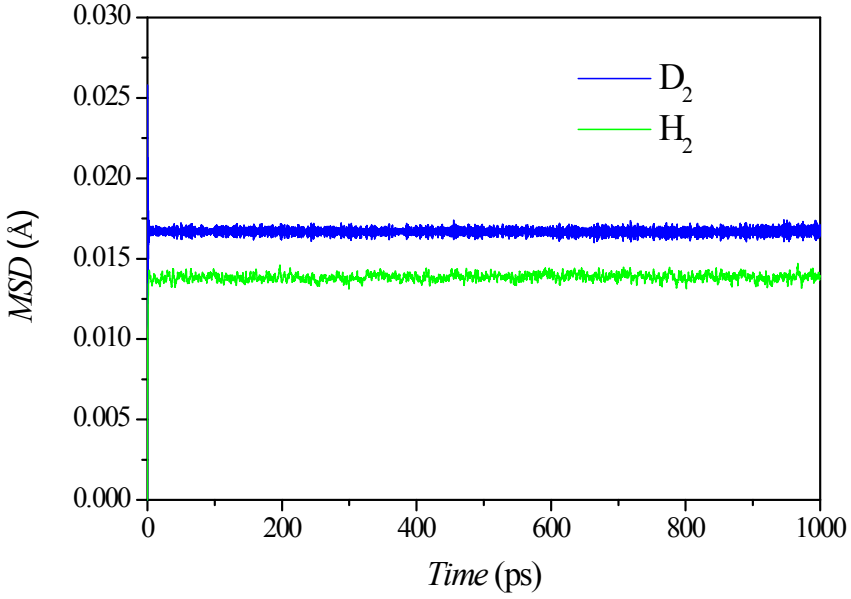


**Figure S8.** The MD-simulated time dependence of the MSD for a single adsorbate molecule in the type–I pore of MOF-EIA (see Figure S7) at 60 K.

## S4.3 Center of mass probability distributions

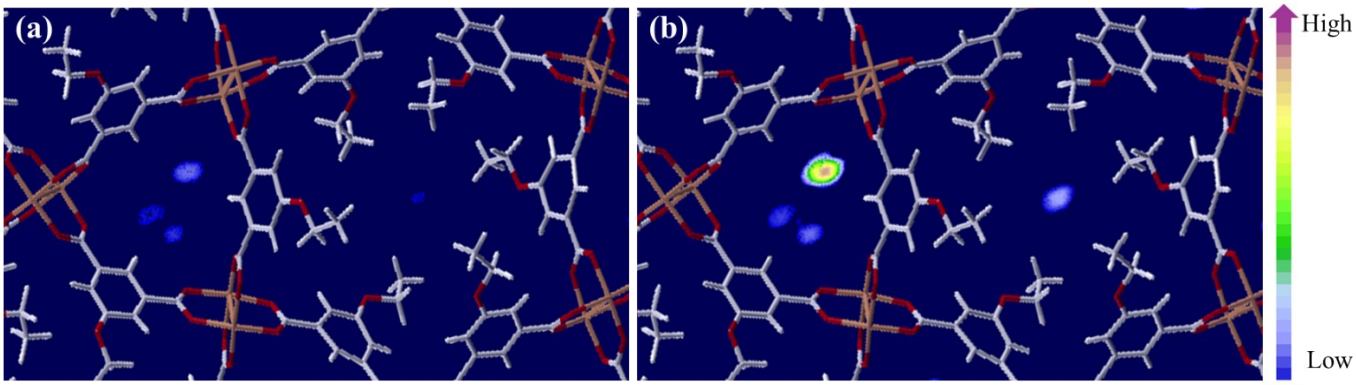


**Figure S9.** Contour plots of the center of mass (COM) probability distribution of $H_2$ (a) and $D_2$ (b) in the mixture adsorbed in MOF-EIA under the conditions of 60 K and 10 kPa. The framework atoms and bonds of the MOF structure are displayed in a stick style for clarity.

## References:


1. B. Garai, A. Mallick, A. Das, R. Mukherjee and R. Banerjee, *CHEM-EUR J*, 2017, **23**, 7361-7366.
2. M. Kondo, T. Okubo, A. Asami, S. Noro, T. Yoshitomi, S. Kitagawa, T. Ishii, H. Matsuzaka and K. Seki, *ANGEW CHEM, INT ED ENGL*, 1999, **38**, 140-143.
3. Y. Kubota, M. Takata, R. Matsuda, R. Kitaura, S. Kitagawa, K. Kato, M. Sakata and T. C. Kobayashi, *ANGEW CHEM, INT ED ENGL*, 2005, **44**, 920-923.
4. Y. Pan, Y. Liu, G. Zeng, L. Zhao and Z. Lai, *CHEM COMMUN*, 2011, **47**, 2071-2073.
5. D. Cao, H. Huang, Y. Lan, X. Chen, Q. Yang, D. Liu, Y. Gong, C. Xiao, C. Zhong and S. Peng, *J MATER CHEM A*, 2018, **6**, 19954-19959.
6. J. F. Fernandez, F. Cuevas and C. Sanchez, *J ALLOY COMPD*, 2000, **298**, 244-253.
7. F. von Zeppelin, M. Haluška and M. Hirscher, *THERMOCHIM ACTA*, 2003, **404**, 251-258.
8. B. Panella, M. Hirscher and B. Ludescher, *MICROPOR MESOPOR MAT*, 2007, **103**, 230-234.
9. D. Cao, S. Peng, X. Chen, J. Hou, P. Chen, C. Xiao, Y. Gong and H. Wang, *ANAL METHODS-UK*, 2017, **9**, 3067-3072.
10. S. A. Fitzgerald, K. Shinbrough, K. H. Rigdon, J. L. C. Rowsell, M. T. Kapelewski, S. H. Pang, K. V. Lawler and P. M. Forster, *J PHYS CHEM C*, 2018, **122**, 1995-2001.
11. I. Krkljus, T. Steriotis, G. Charalambopoulou, A. Gotzias and M. Hirscher, *CARBON*, 2013, **57**, 239-247.
12. H. Oh and M. Hirscher, *EUR J INORG CHEM*, 2016, **2016**, 4278-4289.
13. J. Y. Kim, H. Oh and H. R. Moon, *ADV MATER*, 2019, **31**, 1805293.
14. H. Oh, Max Planck Institute for Intelligent Systems, Stuttgart, 2014.
15. H. Oh, S. B. Kalidindi, Y. Um, S. Bureekaew, R. Schmid, R. A. Fischer and M. Hirscher, *ANGEW CHEM, INT ED ENGL*, 2013, **52**, 13219-13222.
16. J. Teufel, H. Oh, M. Hirscher, M. Wahiduzzaman, L. Zhechkov, A. Kuc, T. Heine, D. Denysenko and D. Volkmer, *ADV MATER*, 2013, **25**, 635-639.
17. G. Han, Y. Gong, H. Huang, D. Cao, X. Chen, D. Liu and C. Zhong, *ACS APPL MATER INTER*, 2018, **10**, 32128-32132.
18. R. Rodríguez-Cantano, R. Pérez De Tudela, M. Bartolomei, M. I. Hernández, J. Campos-Martínez, T. González-Lezana, P. Villarreal, J. Hernández-Rojas and J. Bretón, *J PHYS CHEM A*, 2016, **120**, 5370-5379.
19. F. Darkrim and D. Levesque, *J CHEM PHYS*, 1998, **109**, 4981-4984.
20. S. L. Mayo, B. D. Olafson and W. A. Goddard, *J PHYS CHEM*, 1990, **94**, 8897-8909.
21. T. A. Manz and D. S. Sholl, *J CHEM THEORY COMPUT*, 2012, **8**, 2844-2867.
22. G. Kresse and J. Hafner, *PHYS REV B*, 1993, **47**, 558-561.
23. G. Kresse and J. Furthmüller, *PHYS REV B*, 1996, **54**, 11169-11186.
24. Q. Yang, D. Liu, C. Zhong and J. Li, *CHEM REV*, 2013, **113**, 8261-8323.
25. J. Perdew, K. Burke and M. Ernzerhof, *PHYS REV LETT*, 1996, **77**, 3865-3868.
26. S. Grimme, S. Ehrlich and L. Goerigk, *J COMPUT CHEM*, 2011, **32**, 1456-1465.
27. P. E. Blöchl, *PHYS REV B*, 1994, **50**, 17953-17979.
28. G. Kresse and D. Joubert, *PHYS REV B*, 1999, **59**, 1758-1775.
29. Monkhorst, H. J., Pack and J. D., *PHYS. REV. B*, 1976, **13**, 5188-5192.
30. M. E. Tuckerman, J. Alejandre, R. López-Rendón, A. L. Jochim and G. J. Martyna, *J PHYS A-MATH GEN*, 2006, **39**, 5629-5651.
31. T. F. Miller, M. Eleftheriou, P. Pattnaik, A. Ndirango, D. Newns and G. J. Martyna, *J CHEM PHYS*, 2002, **116**, 8649-8659.